

**LIQUID EFFECT ON SINGLE  
CONTACTED CARBON  
NANOTUBES GROWN BY  
CHEMICAL VAPOR DEPOSITION**  
INAUGURALDISSERTATION

zur

Erlangung der Würde eines Doktors der  
Philosophie vorgelegt der  
Philosophisch-Naturwissenschaftlichen  
Fakultät der Universität Basel

von

Soufiane Ifadir aus Marrakech (MOR)  
D.E.A de Physique de la matière condensée, Strasbourg

Basel, May 2005

22nd April 2005

Genehmigt von der Philosophisch-Naturwissenschaftlichen Fakultät auf  
Antrag der Herren Professoren:  
Prof. Dr. C. Schönenberger  
Prof. Dr. L. Schlapbach  
Prof. Dr. A. Hartschuh  
Prof. Dr. E. Meyer  
Basel, den x. May 2005

# Contents

<b>1</b>	<b><i>Introduction</i></b>	<b>4</b>
1.1	Physics and Nanotechnology . . . . .	4
1.2	Carbon Nanotubes for Nanotechnology . . . . .	4
1.3	Outline . . . . .	5
<b>2</b>	<b><i>Carbon Nanotubes Structure</i></b>	<b>7</b>
2.1	Introduction . . . . .	7
2.2	Electronic Structure of Carbon Nanotubes . . . . .	7
2.2.1	Band Structure of Graphene . . . . .	7
2.2.2	The Lattice of Carbon Nanotubes . . . . .	9
2.2.3	Carbon Nanotubes Band Structure . . . . .	12
2.3	Mesoscopic Transport . . . . .	13
<b>3</b>	<b><i>Carbon Nanotubes Growth</i></b>	<b>16</b>
3.1	Carbon Nanotube Synthesis . . . . .	17
3.2	Chemical Vapor Deposition of Carbon Nanotubes . . . . .	17
3.2.1	Si/SiO <sub>2</sub> Substrate . . . . .	18
3.2.2	Growth on Quartz Substrate . . . . .	22
3.2.3	Growth Mechanism . . . . .	23
3.3	Discussion . . . . .	24
3.4	Conclusion . . . . .	25
<b>4</b>	<b><i>Electrical Characterization of CNT in Air</i></b>	<b>27</b>
4.1	Field Effect . . . . .	28
4.2	Device Fabrication . . . . .	29
4.2.1	Si/SiO <sub>2</sub> Substrate . . . . .	29
4.2.2	Quartz Substrate . . . . .	30
4.3	Room Temperature Characteristics . . . . .	30

---

4.3.1	Si/SiO <sub>2</sub> FET . . . . .	31
4.3.2	Quartz FET . . . . .	33
4.4	Conclusion . . . . .	34
<b>5</b>	<b><i>Carbon Nanotubes in Liquids</i></b>	<b>36</b>
5.1	Unconventional Gating . . . . .	37
5.1.1	Planar Gates . . . . .	37
5.1.2	Electrochemical Gate . . . . .	38
5.2	Carbon Nanotube in an Organic Solution . . . . .	39
5.2.1	NT in Aromatic Compound . . . . .	40
5.2.2	NTFET in Liquid Crystal . . . . .	44
5.3	Possible Applications . . . . .	46
<b>6</b>	<b><i>Outlook and Conclusion</i></b>	<b>47</b>
<b>7</b>	<b><i>Appendix</i></b>	<b>48</b>
7.1	Chemical Vapor Deposition Growth Parameters . . . . .	48
7.2	Shell Burning . . . . .	49
7.3	CNFET in Aromatic . . . . .	50
7.4	Additional Liquid Crystal Measurements . . . . .	51
<b>8</b>	<b><i>Acknowledgement</i></b>	<b>52</b>

# Chapter 1

## *Introduction*

### 1.1 Physics and Nanotechnology

The convergence of experimental sciences toward studying objects at nanometer scale promoted the definition of a new discipline: nanotechnology. This word tends to screen even the word Physics which is actually the more true and general. Nanotechnology is rather a branch more coherent with industrial progress and the course to the Very Low Scale Integration (VLSI). In any case, nanotechnology is a challenging and interesting domain providing at the same time the emergence of new technologies in daily life and a look at beauty of physics in nano-scale.

### 1.2 Carbon Nanotubes for Nanotechnology

In nature, material exists under different form ranging from highly disordered systems (gas) to highly ordered (crystals). Carbon element exists under a disordered state (amorphous) and an ordered state (graphite and diamond). A new forms of carbon: fullerene and carbon nanotubes were discovered by Kroto [1] in 1985 and by Iijima in 1991, respectively [2]. This new form of compacted carbon revolutionize the research. Fullerene and Carbon Nanotube are indeed excellent candidates for the ultra low scale integration technology and basic research in Mesoscopic Physics.

The reduced dimensionality of Carbon Nanotubes (CNTs) provides interesting physical properties. CNTs have a Young modulus reaching 1 TPa [3] and can be ballistic electrical conductors [4].

Carbon nanotubes are hollow cylinders material of diameter ranging from 1 nm (mono-shell carbon or Single Wall Carbon Nanotube (SWCNT)), to more than 10 nm (multi-shell or MultiWall Carbon Nanotube (MWCNT)). The arrangement of the carbon atoms among the shell provide different chirality to carbon nanotubes (ie: the atomic arrangement and hence the atomic orbitals overlaps). Depending on the chirality, carbon nanotubes can be semiconductors or metals.

Carbon nanotubes have the ‘right’ combination of properties: nanometer size diameter and high aspect ration, structural integrity, high electrical conductivity, and chemical stability. These properties open a wide spectrum of applications like electron emitters [5], hydrogen storage owing to the extraordinarily high and reversible hydrogen adsorption in SWNT [6]. In Atomic Force Microscopy they can provide ultra-thin high resolution and robust tips [7]. In the area of sensing, field-effect transistors (FETs) devices with SWCNTs as the conducting channel can be used as chemical sensors. The interest in nanotube-FETs lies in their potential to perform better than conventional silicon based FETs. Parameters such as mobility and transconductance dictate the performance of a FET.

Intrinsic channel mobility in the range of  $20.000 \text{ cm}^2/\text{Vs}$  for CNFETs have been reported [8], compared with  $500 \text{ cm}^2/\text{Vs}$  for Si MOSFETS. Furthermore, CNFETs have also been shown to have significantly higher transconductance, the measure of current carrying capability of FETs. High transconductance implies that the transistors can operate faster. Along with their small size and versatility as chemical and molecular sensors, nanotubes certainly have several advantages over silicon for future nanoelectronics. The electronic properties of single-walled carbon nanotubes are shown to be extremely sensitive to the chemical environment [9]. Nanotube based chemical and molecular sensors have also been reported by [10].

## 1.3 Outline

The goal of this work is to study the electron transport in carbon nanotubes grown by chemical vapor deposition in different liquid media. Chapter 2 is devoted to an introduction to the structural properties of carbon nanotubes necessary to understand their electrical transport. The second chapter is a description of the nanotube production with different catalysts with some

insight into the growth mechanism. Chapter 3 is devoted to the room temperature characterization of grown carbon nanotubes. Finally, in the last chapter we will see how those nanotubes behave in various liquids.

# Chapter 2

## *Carbon Nanotubes Structure*

### 2.1 Introduction

The understanding of the electronic properties of carbon nanotubes is crucial before investigating any application possibilities. In this chapter, we will explain how the electronic structure is correlated to the electrical transport properties of carbon nanotubes. Some useful concepts of Mesoscopic Physics will be exposed.

### 2.2 Electronic Structure of Carbon Nanotubes

The electronic structure of a CNT is simply that of two-dimensional graphite with the additional periodic boundary condition in the circumferential direction. This boundary condition leads to the quantization of the wave vector along the circumferential direction while the translational wave vector remain continuous (infinite tube).

#### 2.2.1 Band Structure of Graphene

A graphene sheet is a two dimensional carbon crystallizing in an hexagonal lattice. The C-C bond is an  $sp^2$  hybridization of the  $2s$ ,  $2p_x$  and  $2p_y$  single atomic wave functions called  $\sigma$  bonds belonging to the graphene  $xy$  plane. A second  $\pi$  bond is formed out of plane by the overlap of the remaining  $2p_z$  orbitals (Wallace problem)[11].

The  $\pi$  electrons are valence electrons. The understanding of the  $\pi$  energy

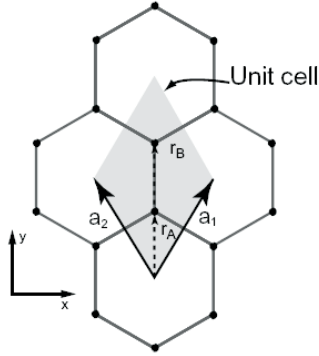


Fig. 2.0: A hexagonal lattice with the lattice vectors  $\mathbf{a}_1$  and  $\mathbf{a}_2$ , the grey area corresponds to one choice of unit cell,  $\mathbf{r}_A$  and  $\mathbf{r}_B$  points to the two atoms in the unit cell.

level is important and relevant for transport and chemical reactivity of carbon nanotubes.

The Bravais lattice is hexagonal and the unit cell contains two carbon atoms (Fig 2.0) described by two unit vectors,  $\mathbf{a}_1$  and  $\mathbf{a}_2$  with coordinates  $(\sqrt{3}a/2, \pm a/2)$ . The C-C bond length is  $1.42\text{\AA}$  which give a unit vector length of  $a = \sqrt{3} \times 1.42\text{\AA} = 2.46\text{\AA}$ .

The dispersion relation for the  $\pi$ -electrons of the graphene in the tight-binding approximation is [12]

$$E(k_x, k_y) = \pm\beta\sqrt{[1 + 4\cos(\frac{\sqrt{3}k_x a}{2}) + \cos(\frac{k_y a}{2}) + 4\cos^2(\frac{k_y a}{2})]} \quad (2.1)$$

Where  $\beta$  is the energy *overlap integral* between nearest neighbors, (+) is the anti-bonding band and (-) is the bonding band.

The Brillouin zone of two-dimensional graphite is shown as the shaded area in Figure 2.1 where  $\Gamma$ ,  $K$ ,  $K'$  and  $M$  represent points of high symmetry. The reciprocal unit vectors are given by

$$\mathbf{b}_1 = (\frac{2\pi}{a}, \frac{2\pi}{\sqrt{3}a}), \mathbf{b}_2 = (-\frac{2\pi}{a}, \frac{2\pi}{\sqrt{3}a}) \quad (2.2)$$

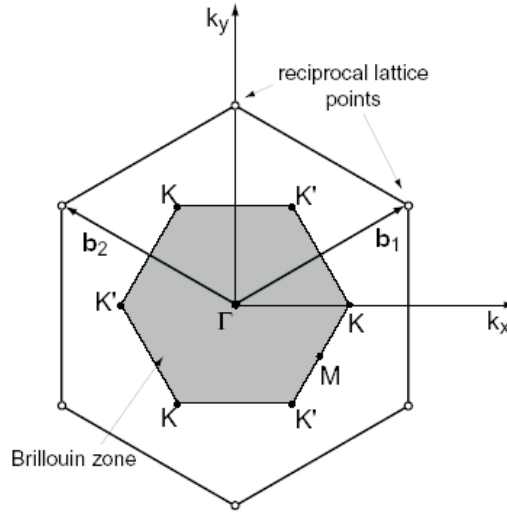


Figure 2.1: the reciprocal lattice point and the Brillouin zone for graphene, with its high symmetry points.  $\mathbf{K}$  and  $\mathbf{K}'$  are the points where the  $\pi$  and  $\pi^*$  dispersion bands is touching each other. The three  $\mathbf{K}$  points are equivalent since they are connected by the reciprocal lattice vectors  $\mathbf{b}_1$  and  $\mathbf{b}_2$ . Since the points  $\mathbf{K}$  and  $\mathbf{K}'$  cannot be connected by the reciprocal lattice vectors these point are not equivalent.

### 2.2.2 The Lattice of Carbon Nanotubes

The single sheet or single wall carbon nanotube can be thought as rolling up a single graphite sheet (graphene).

#### The chiral vector

To figure out how the nanotube is rolled up, we define a chiral vector  $\mathbf{C}$ . This vector is shown in Figure 2.2 and is defined by

$$\mathbf{C} = n\mathbf{a}_1 + m\mathbf{a}_2 \quad (2.3)$$

where  $n, m$  integers with  $0 < |m| < n$ .

$\mathbf{C}$  defines the two points in the graphite sheet that are joined together when we roll the sheet into a carbon nanotube. From this we see that the indices  $(n, m)$  actually uniquely define the nanotube.

Due to the symmetry of the hexagonal lattice, we can choose  $\theta$  between  $0^\circ$

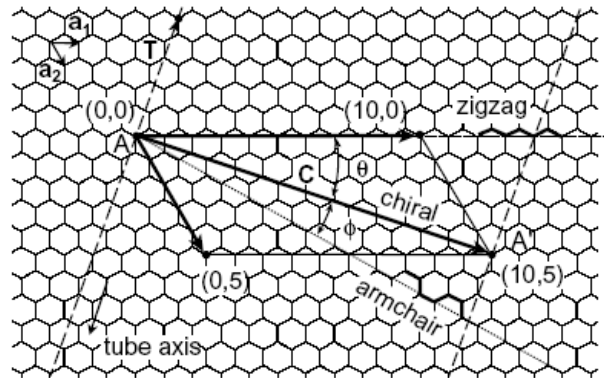


Figure 2.2: A graphene sheet is rolled up to form a (10,5) nanotube by connecting the dashed lines along vector  $\mathbf{C}$ . The wrapping angle of chiral tubes are specified relative to the zigzag ( $\theta$ ) or armchair ( $\phi = 30^\circ - \theta$ ) direction. Also shown is the lattice vector  $\mathbf{T}$  of the 1D unit cell.

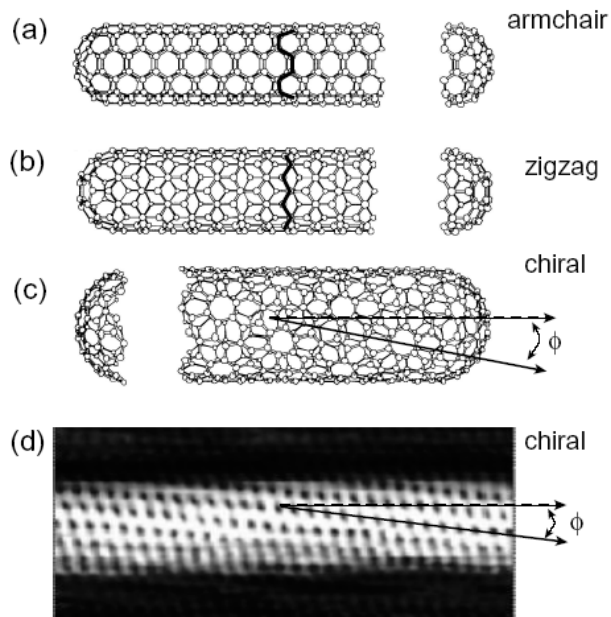


Figure 2.3: (a-c) Shown are a (5,5) armchair tube, a (9,0) zigzag tube, and a (10,5) chiral tube which has been constructed. (d) Atomically resolved STM image of an individual single-wall carbon nanotube. The diameter here was found to be  $d = 1.3$  nm and the chiral angle  $\phi = 7$  [13].

and  $30^\circ$ . The norm of  $\mathbf{C}$  is equal to the circumference length of the nanotube so that the diameter  $d$  of the tube is

$$d = \frac{|\mathbf{C}|}{\pi}, |\mathbf{C}| = a\sqrt{n^2 + m^2 + nm} \quad (2.4)$$

and the chiral angle

$$\cos(\phi) = \frac{2n + m}{2\sqrt{n^2 + m^2 + nm}} \quad (2.5)$$

The tube can be characterized by the set  $(n,m)$  or alternatively by the chiral angle and the diameter  $(\phi,d)$  which is the standard convention for the tubes.

Special symmetry directions in the graphene lattice are  $(n,0)$  and  $(n,n)$  which are called the zigzag and armchair direction, respectively. Figure 2.3 shows schematic examples of an armchair, a zigzag and a chiral tube together with a scanning tunnelling microscopy image of an individual single-wall carbon nanotube [13].

### The translation vector

The translation vector  $\mathbf{T}$  describes how far we should move along the nanotube before the pattern of the carbon atoms on the nanotube repeats itself and it therefore defines the length of the nanotube unit cell.  $\mathbf{T}$  is defined by:

$$\mathbf{T} = s\mathbf{a}_1 + t\mathbf{a}_2 \quad (2.6)$$

Since  $\mathbf{T} \cdot \mathbf{C} = 0$  we obtain the relation (for the smallest  $|T|$ )

$$s = \frac{2n + m}{d_c}, t = \frac{-(2n + m)}{d_c} \quad (2.7)$$

Where  $d_c$  is the greatest common divisor (gcd) of  $2n+m$  and  $2m+n$ .

We have now characterized only single wall nanotubes for simplicity. For the multiwall nanotubes each layer has its particular  $(n,m)$  and eventually the inter-wall interaction can be relevant for establishing a similar formalism for the multiwalls.

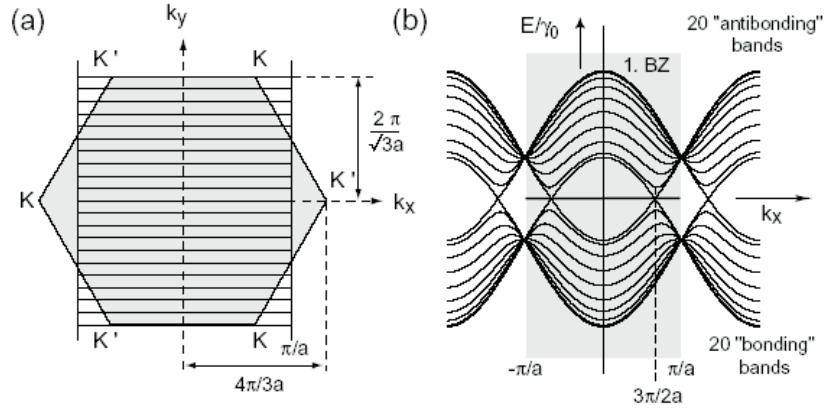


Figure 2.4: (a) An illustration Brillouin zone of graphene (gray areas). The black lines shows allowed wave vectors . (b) Bandstructure of the (10,10) armchair nanotube. The shaded region is the first Brillouin zone.

### 2.2.3 Carbon Nanotubes Band Structure

From the translation and chiral vectors we can construct the reciprocal lattice vectors. Since there are  $2N$  atoms in the unit cell this should lead to  $N$  pairs of  $\pi$ -bonding and  $\pi$ -anti-bonding bands.

The reciprocal lattice vectors  $\mathbf{K}_1$  and  $\mathbf{K}_2$  for a carbon nanotube are defined by the following relations

$$\mathbf{C} \cdot \mathbf{K}_1 = 2\pi, \mathbf{C} \cdot \mathbf{K}_2 = 0 \quad (2.8)$$

$$\mathbf{T} \cdot \mathbf{K}_1 = 0, \mathbf{T} \cdot \mathbf{K}_2 = 2\pi \quad (2.9)$$

With the use of this equation, eq(1.6) and eq(1.7) a simple calculation yields

$$\mathbf{K}_1 = \frac{1}{N}(-t\mathbf{b}_1 + s\mathbf{b}_1), \mathbf{K}_2 = \frac{1}{N}(m\mathbf{b}_1 - n\mathbf{b}_1) \quad (2.10)$$

Where  $\mathbf{b}_1$  and  $\mathbf{b}_2$  are the reciprocal lattice vectors for graphite.

Due to the periodic boundary condition, the only allowed wave vector components in the circumferential direction are those that obey  $\mathbf{C} \cdot \mathbf{k} = 2\pi l$ , where  $l$  is an integer. The vectors that fulfill this requirement are those whose circumferential component is a multiple of  $\mathbf{K}_1$ .

In Figure 2.4 the allowed states for an electron in a nanotube are indicated by the black lines on a background of the reciprocal lattice of graphene

where the light-grey hexagon indicate the Brillouin zone graphene.

The dispersion relation can now be found by slicing the dispersion relation for graphene along the lines with allowed wave vectors that are seen as black lines. These black lines indicating the allowed states are given by:

$$\mathbf{k} = l_1 \mathbf{K}_1 + l_2 \frac{\mathbf{K}_2}{|\mathbf{K}_2|}; \frac{-\pi}{T} < l_2 < \frac{\pi}{T}, l_1 = 0, 1, \dots, N-1 \quad (2.11)$$

If one of these slices happens to cut through the  $\mathbf{K}$  point the nanotube will be metallic and if the slice does not cut through a  $\mathbf{K}$  point it will be semiconducting.

The density of states of all metallic nanotubes

$$N(E_F) = \frac{8}{\sqrt{3}\pi a\beta} \quad (2.12)$$

Concerning the semiconducting tubes, their energy gap depends on the reciprocal tube diameter

$$E_g = \frac{\beta a}{d} \quad (2.13)$$

This value is independent of the chiral angle.

## 2.3 Mesoscopic Transport

The Greek word meso stands for intermediate. Mesoscopic phenomena are those standing between the macro (bulk) and the micro (atom) world. It is the regime where wave function propagate coherently over mesoscopic distances.

The classical physical description in mesoscopic scale is not valid as the dimensions starts to be comparable to characteristic lengths of the electronic wave function. Electron transport, for example, can not be described by the Drude model and the following expression of the conductivity is in general only approximately valid[14]:

$$\sigma = \frac{ne^2\tau^{coll}}{m} \quad (2.14)$$

where  $\tau^{coll}$  is the carrier collision relaxation time,  $n$  the density and  $m$  the mass of the carriers.

In the Drude picture, (*classical* regime) it is assumed that all single scattering events due to impurities are incoherent. *Ballistic* regime can take place if the transit time during which the electron traverse the sample is smaller than the momentum relaxation time. For ballistic transport, the total current  $I$  from a region where the chemical potential is  $\mu_1$  to a one with a chemical potential  $\mu_2$  is given by:

$$I = \frac{2e^2}{h} M \frac{\mu_1 - \mu_2}{e} \quad (2.15)$$

Where  $M$  is the total conduction channels. A channel stands for the subbands which have wave vectors states in the energy range such  $\mu_1 < E < \mu_2$ .

The resistance  $R_c$  and the conductance  $G_c$  of a ballistic conductor are given by:

$$R_c = \frac{(\mu_1 - \mu_2)/e}{I} \quad (2.16)$$

$$= \frac{h}{2e^2} \cdot \frac{1}{M} \quad (2.17)$$

$$G_c = G_0 M \quad (2.18)$$

$$G_0 = \frac{2e^2}{h} \quad (2.19)$$

$R_c$  is the contact resistance and  $R_0$  is the quantum resistance defined as:

$$R_0 = \frac{h}{2e^2} \simeq 12.5k\Omega. \quad (2.20)$$

Thus in a wire with no scattering the conductance is proportional to  $M$ . The quantized conductance can be seen in a clean semiconductors at low temperatures.

When we consider static scattering, that is scattering by a potential in one dimension, the conductance can be deduced from Eq. 2.18 by taking into account the transmission probability  $\Gamma$  for a channel to go from one electrode to another. The transmission is given by the sum of transmission probabilities from  $i$ th to  $j$ th channel,  $t_{ij}$ :

$$G = \frac{2e^2}{h} M\Gamma = \frac{2e^2}{h} \sum |t_{ij}|^2 \quad (2.21)$$

$$R = \frac{h}{2e^2} \frac{1}{M\Gamma}; \Gamma = \sum |t_{ij}| \quad (2.22)$$

The resistance of a wire  $R_w$  for a single channel is given in terms of the transmission probability  $\Gamma$  as

$$R_w = R - R_c \quad (2.23)$$

$$= R_0 \frac{1 - \Gamma}{\Gamma} \quad (2.24)$$

The measurement of the contact resistance can tell about the quality of the contact and the number of channels involved in transport. It is related to the amount and the nature of the impurities present in the structure. Changing or perturbing the transmission probabilities  $t_{ij}$  can have a dramatic effect on the band structure and hence on the transport.

The facility about which the carrier drift in a conductor is related microscopically to  $\Gamma$  and macroscopically described by the mobility  $\mu$  which is the ration between the drift velocity  $v$  and the applied electrical filed  $E$ :  $\mu = \frac{v}{E}$ . If  $m$  is the carrier mass and  $q$  the charge, the mobility can be written as:

$$\mu = \frac{q\tau^{coll}}{m} \quad (2.25)$$

The mobility is expected to be large for smaller mass or large scattering times.

Impurity scattering and lattice scattering affect its value. In carbon nanotubes all carbon atoms are located on the surface and the  $\pi$  wave functions extend away from the surface. The adjacent layer of the surface affect the surface. The mobility is influenced by a combination effects of both layers. The presence of charged surface states or ionized impurity reduces the mobility which can be seen in the value of the resistance.

# Chapter 3

## *Carbon Nanotubes Growth*

In this chapter we will present the growth of carbon nanotubes with different procedures. Mainly, we will see that for different type of catalyst the growth result will be different. Certain aspects of the growth mechanism will be discussed.

## 3.1 Carbon Nanotube Synthesis

Carbon Nanotubes (CNTs) were discovered by Iijima in the soot of an arc-discharge chamber. This method has been used to produce carbon fibers (SWCNTs, MWCNTs) and fullerenes. Bundled CNTs with small diameter were also produced by laser ablation [15]. A third method consisting of catalytic growth of CNTs was discovered by Yacaman [16].

There exist three methods for synthesizing CNTs:

- Arc discharge: nanotubes are grown on the negative end of a carbon electrode used for the direct current arc discharge in an argon filled vessel. The tubes (MWCNTs) obtained are ranging from 4 to 30 nm in diameter and up to  $1\mu\text{m}$  length. The carbon is sublimated in the reactor while reaching a temperature above  $3000^\circ\text{C}$ .
- Laser ablation: In 1996, Smalley and coworkers produced high yield (70%) of single wall carbon nanotube (SWCNT) by laser ablation of graphite rods with a small amount of Ni and Co at  $1200^\circ\text{C}$ . These method provides high yield of SWCNT in the presence of a metallic catalyst (Ni and Co). Ropes of 5 to 20 nm in diameter with apparent dominant chirality (10,10) and hundreds of microns long are grown. A further procedure of isolation and purification is required for this type of growth.
- Catalytic growth: a more 'efficient' approach to produce NTs is the Chemical Vapor Deposition (CVD) or catalytic growth. NTs are grown by thermal decomposition of hydrocarbon gases. The details of CVD are given in the next section.

## 3.2 Chemical Vapor Deposition of Carbon Nanotubes

The easiest way to obtain CNT, is by the catalytic Chemical Vapor Deposition (CVD). CVD is a physicochemical process consisting of the decomposition of hydrocarbon gases at high temperature ( $600^\circ\text{C}$  -  $1000^\circ\text{C}$ ) in the presence of catalyst (Ni, Fe, etc).

In comparison to the laser ablation and arc discharge tubes, the CVD tubes do not require very high temperatures and further steps of purification from

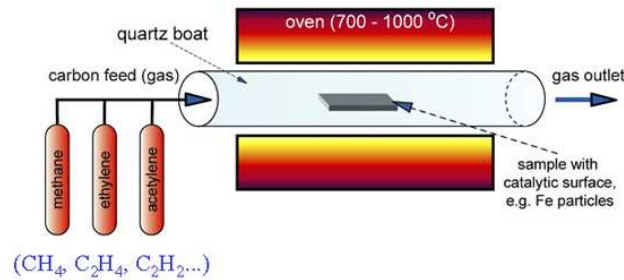


Figure 3.1: Chemical Vapor Deposition oven

amorphous carbon and diverse nanoparticles. The CVD tubes are also easier to be addressed on a surface (electrical contacting) and do have rather small diameter dispersions [17]. Fig. 3.1 is schematic of the oven we use to grow our tubes.

### 3.2.1 Si/SiO<sub>2</sub> Substrate

Si/SiO<sub>2</sub> (400 nm oxide thickness substrates) are used as a template for growing the tubes. In our experiments, we used three different catalyst: ferritin, layer evaporated iron and an iron nitrate based solution.

#### 1. *evaporated iron*

UV lithography is used to pattern a Si/SiO<sub>2</sub> substrate with an evaporated iron layer. The iron evaporation is realized at pressures of the order of 10<sup>-5</sup>mbar. The growth results show two types of tubes depending on the thickness of the iron layer:

- Vertical growth: the film thickness is 5 nm (Fig. 3.2). The growth results of perpendicular tubes to SiO<sub>2</sub> surface. For such a thickness, the iron catalytic centers have a high density and lead to high density tubes. The nanotubes have spatially only one degree of freedom in which they can grow, namely perpendicular to the surface [18]. The tubes are very compact which assures a mechanical stability of a vertical structure.
- Planar growth: 5 Å thickness of evaporated iron is used as catalyst. This thickness results in formation of non continuous film

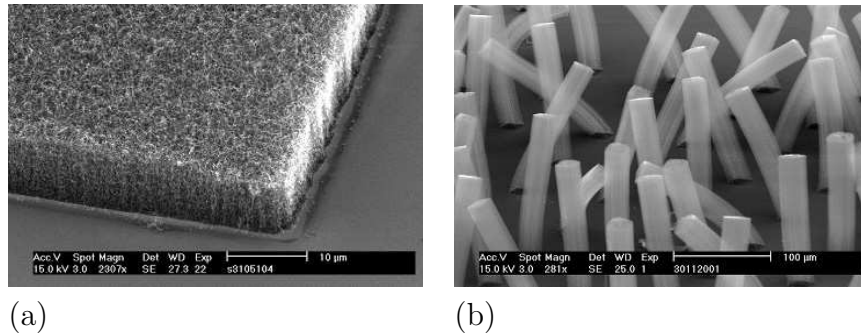


Figure 3.2: Growth from evaporated iron layer. (a) vertical growth, scale (10  $\mu\text{m}$ ). (b) some vertical bundle tend to fall due to mechanical instability, scale (100  $\mu\text{m}$ ) (Z. Liu et al).

with iron clusters. The low density clusters lead to planar nanotubes, the tubes look straight with kinks sometimes indicating the presence of defects.

The simple observations above imply that the type of growth depends on the catalyst cluster size. One can control the growth type by simply tuning the catalyst clusters size.

## 2. *Ferritin as catalyst*

Some organic compounds which carry simultaneously apolar and polar chemical groups exhibit self assembly. This property can be exploited for fundamental studies (2D solid state physics) and for engineering purposes at the nanoscale.

Positioning a nanotube at specific locations can be of big importance for different type of applications. By positioning catalyst sites at different locations, one can hope to grow tubes locally.

The possibility of ferritin to self assemble [19] combined with its the ability to carry a catalytic center with tunable size provides a good tool to place one or an assembly of nanotubes at specific locations.

We used ferritin as a catalyst for our growth. Ferritin is composed of 24 polypeptide subunits, which are arranged to form a nearly spherical

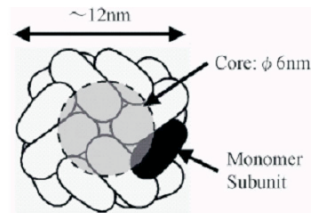


Figure 3.3: Ferritin and its spherical like structure

hollow shell with outside and inside diameter of 12 and 8 nm [20]. The polypeptide shell can store up to 4500 iron atoms forming an *iron oxide core* (Fig. 3.3).

A piece of Si/SiO<sub>2</sub> wafer is spin coated (4000 tr/min) during 40 s with a few milliliters ferritin solution at a concentration of 10 mg/ml diluted in water from the stock solution (40 mg/ml, F-7879 from SIGMA). The sample is flushed with argon under 1000 cm<sup>3</sup>/min while reaching 750° C followed by introduction of hydrogen 600 cm<sup>3</sup>/min for 5 min and acetylene 20 cm<sup>3</sup>/min for 10 min.

The growth leads to two type of nanostructures: MWCNT (Fig. 3.4 (a)), small fibers (Fig. 3.4 (b)) and coiled carbon nanostructures (Fig. 3.5).

The fact that ferritin protein carries a diversity of chemical species (N,H,O...) and the intermediate iron cluster density on the surface may make favorable the growth of coiled out of plane composite (C,N,...) nanostructures as shown in the figures. The effect of the size (length and thickness) is probably responsible for that coiled structure adopted by the system to minimize its curvature energy.

### 3. *Iron nitrate based solution catalyst particles*

Iron nitrate ((Fe<sub>2</sub>(NO<sub>3</sub>))<sub>3</sub>.9H<sub>2</sub>O, Flucka) nanoparticles suspended in isopropanol and stabilized with molybdenum dichloride dioxide (MoCl<sub>2</sub>O<sub>2</sub>) and alumina (Al<sub>2</sub>O<sub>3</sub>) is used as a solution catalyst for growth. The tubes obtained by this catalyst look straight (SEM) and display good semiconducting behavior (Chap 3.). This catalyst is widely used by the carbon nanotube community and it is the standard one for tube production in our group.

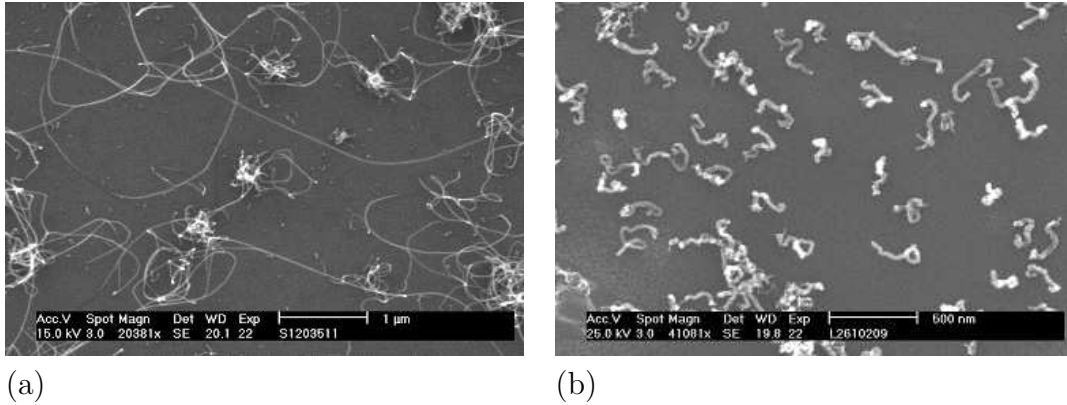


Figure 3.4: SEM pictures of carbon nanotubes grown by CVD with ethylene as feeding gas and Ferritin as catalyst on SiO<sub>2</sub>. (a) The scale bare is 1 μm. (b) the scale bar is 500 nm

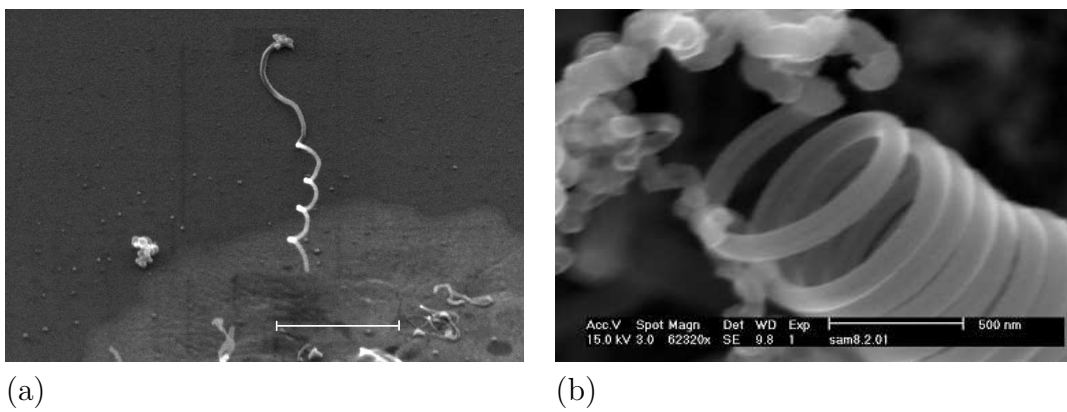


Figure 3.5: Coiled carbon nanostructure grown from ferritin. (a) Scale bare is 1 μm. (b) Scale bare is 500 nm

### 3.2.2 Growth on Quartz Substrate

The Si/SiO<sub>2</sub> substrate is a good substrate for mass production (cost and performances) in semiconductor industry. Recently new generations of transistor has been made on the basis of different substrate due the severe limitations of the silicon based devices (high frequency operating, limited mobility or leakage current). The High Electron Mobility Transistor (HEMT) based on Ga-GaAs is one of the best examples.

Studying the interaction NT - liquid solution is one of the currently active research subject aiming to realize a single molecular sensors. Ultimately, one would like to track a single molecular interaction ‘molecule - NT’ electrically, and bring simultaneously an optical information (fluorescence for example) demonstrating the molecular interaction. The use of a transparent substrate would be ideal for this type of experiments.

Investigating the properties of CNTs using Raman spectroscopy require in addition a transparent substrate.

Another reason for seeking of a new substrate is the occurrence of leakage current to the back gate during electrical measurements of CNT. This leak current limits the performances and arise from the bad isolation of SiO<sub>2</sub> dielectric due to local defects or cracks likely formed during CVD (Chap. (4)). Fabricating devices on transparent and perfectly isolating substrate would be a possible solution.

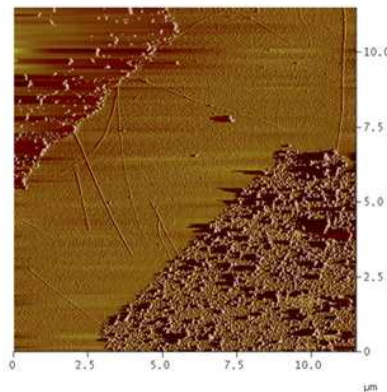


Figure 3.6: AFM picture of NTs on quartz grown with evaporated iron

The substrate we use is a one side polished quartz ( $2 \times 2 \text{ cm}^2$ ) slice with 0.5 mm thickness and 001 (crystal GmbH, Germany). Quartz can sustain high

temperatures necessary for tubes growth. The catalyst used is 5 Å evaporated iron. Fig. 3.6. shows an AFM picture of tubes grown from pre - patterned iron islands.

### 3.2.3 Growth Mechanism

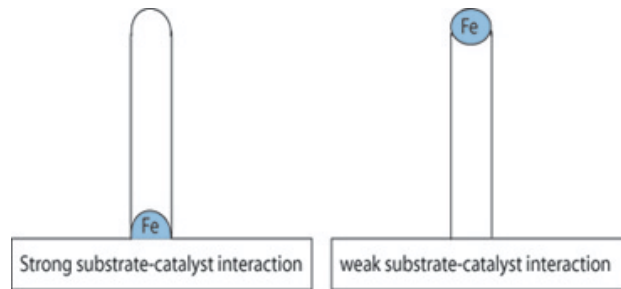


Figure 3.7: Schematic of the base and the tip growth mechanism

It has been established that transition metals catalyst are necessary for the growth of CNTs [17]. The nature of the catalyst, the gas composition, the temperature and the nature of the substrate surface (roughness...) are crucial for the growth result. During CVD reaction, carbon atoms decompose from hydrocarbon are adsorbed on the nanoparticle anchored on the surface substrate forming a carbon iron solution. When the saturation point is reached, carbon starts to assemble leaving the catalyst (base growth) or pushing the catalyst depending on the substrate catalyst interaction (tip growth)[21, 22]. Figure 3.7. illustrates these two proposed mechanisms. The growth terminates when the feeding gas become insufficient or the tube encounter obstacles.

Y.Zhang's [23] observation (Fig. 3.8 (a)) support the idea of the base growth mechanism, consistent with the strong interaction between the catalyst and the substrate. A strong substrate catalyst interaction is also observed in our case while sonicating strongly the samples; No displacement of the tubes has been noticed.

Another aspect of the mechanism of growth is the time needed to obtain tubes with certain length. An estimation of growth time scale in the range of 1-10 micron/s has been observed using the field emission current from the extremity of a nanotube with an activation time of a few seconds [25].

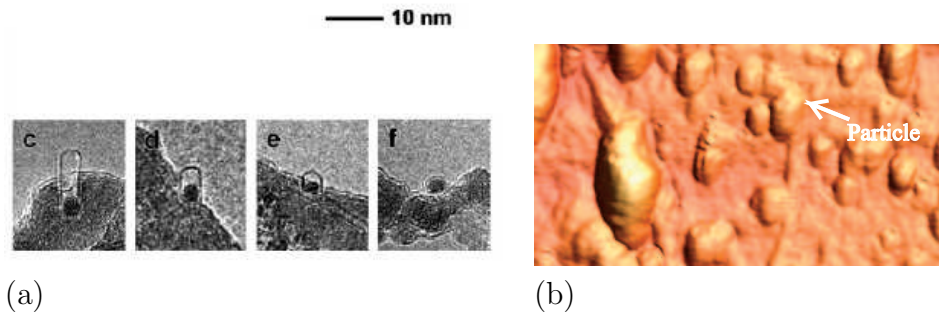


Figure 3.8: Growth from a single particle. (a) TEM illustrating the base growth mechanism [23]. (b) AFM picture of a single tube born from a single nanoparticle [24].

### 3.3 Discussion

The production of nanotubes in a reproducible way is a challenging nanotechnology process. During the growth, although we keep all parameters (flow, temperature, gases composition) constant, we observe a dispersion of the nanotube diameters and lengths. In addition to multiwall CNT, bundled carbon tubes are present. The usual scanning tools used to investigate the surface (SEM, AFM) can bring only a rough and limited information about the quality (diameter, defects,...) of the NT since it can not provide atomic details. The limitation of AFM is illustrated by Fig. 3.9. The single tube and the branched one display the same apparent diameter. Small bundles of tubes and single tubes are indistinguishable.

The AFM is also not very convenient for the next processing steps (electrical contacting Chap. 4.) because it is time consuming, although it can provide precise profile measurements. We prefer to use SEM (with the risk to alter the tube structure) to locate our tubes. We performed a comparative study between SEM and AFM to see if all features can be simultaneously seen (Fig. 3.10). All nanotubes detected by the atomic microscope can also be seen the in SEM. However, a contrast difference is detected with SEM for different tubes which might be attributed to the difference on the electronic structure (chirality).

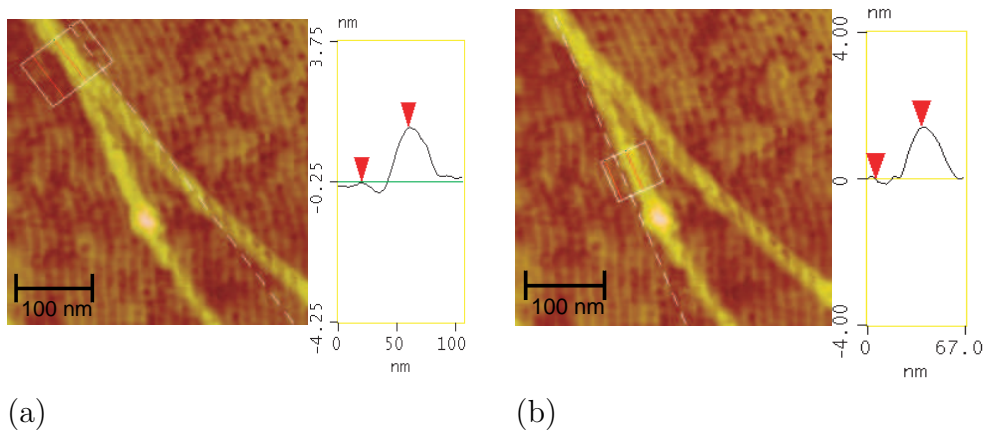


Figure 3.9: AFM pictures of carbon nanotubes grown by CVD  $\text{SiO}_2$ . The diameter of the bundle (a) is 1.6 nm where as the diameter of the lower tube (b) is 1.5 nm

### 3.4 Conclusion

The use of different catalyst results in different carbon nanotube shape and morphology. A systematic way of producing carbon nanotubes is not yet well established. The post growth processing steps remain another step to select the tube according to its size, shape and morphology. Despite the non uniform and non homogeneous tube production, chemical vapor deposition remain a cheap and easy tool to obtain carbon nanotubes.

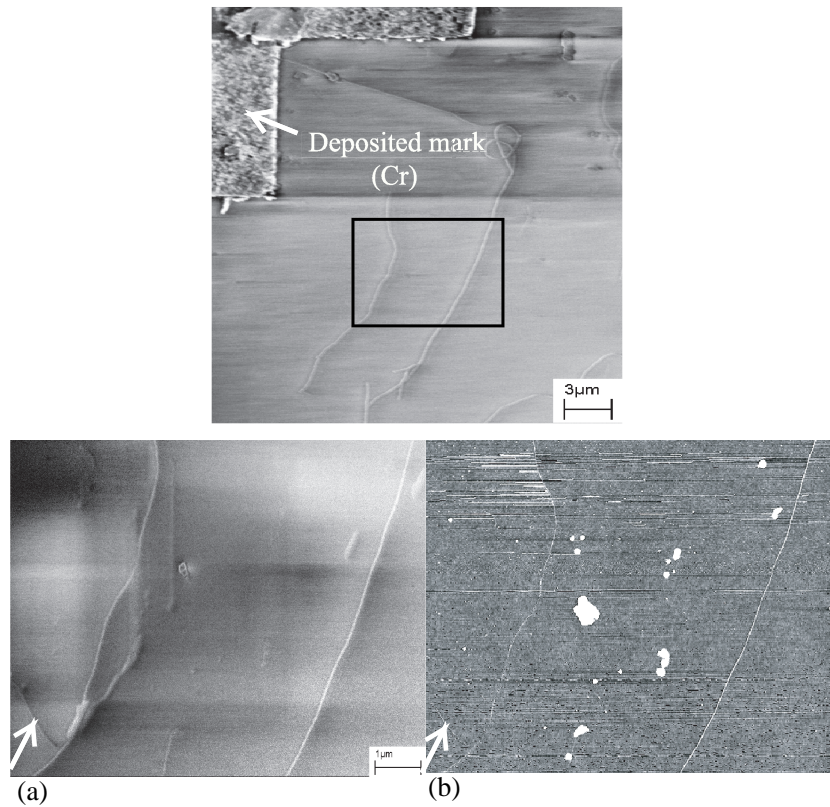


Figure 3.10:

The upper picture is a scan (SEM) of an area close to a marker. The lower figures are SEM and AFM zoom of the squared region, respectively. The AFM picture is better resolved but the SEM picture display all features.

## Chapter 4

# *Electrical Characterization of CNT in Air*

This chapter is devoted to the electrical characterization of CVD grown tubes before studying them in liquid media. As mentioned before, the growth results in a multitude of tubes with very small diameter that can be small bundle, metallic or semiconductor. The gate response is a tool to distinguish semiconducting nanotubes from metallic ones and the estimation of the carrier mobility in the tube provide an idea about the quality of the tube.

## 4.1 Field Effect

The bipolar junction transistor (BJT) and field effect transistor (FET) are the most commonly used transistor configurations. For the case of the BJT, a collector current is controlled by a smaller base current, and the device is modelled as a current-controlled current source. This is in contrast to the FET, where a gate voltage is used to control a drain current, i.e the FET behaves as a voltage - controlled source.

The nanometer size of carbon tubes combined with their intrinsic electrical properties provide the perfect combination to use in nanoelectronics in order to replace the conventional Metal Oxide Semiconductor Field Effect Transistor (MOSFET). In principle one can fabricate a very small Nanotube Field Effect Transistor (NTFET) where the FET channel is a carbon nanotube, the only limitation will come from the limited wavelength of lithography technique used for designing the source and drain electrodes.

FETs belong to the family of two pole circuits. One of the interesting transfer function of this two pole is the transconductance  $g_m$ , which evaluate the degree of modulation of the Source - Drain (S-D) current (or the device conductance) by the applied external electrical field. Assuming that transport in our NTs is diffusive at room temperature and in the linear regime, the transconductance is given by [26]

$$g_m = \frac{dI}{dV_G} = \mu \frac{C}{L^2} V_{SD} \quad (4.1)$$

where  $\mu$  is the carrier mobility,  $C$  is the NT capacitance,  $L$  is the tube length and  $V_{SD}$  is the source - drain voltage. Hence, the electrical measurements can provide an estimate of the mobility and the charge density of the carriers at  $V_G = 0$ . This can be obtained from the threshold voltage  $V_{G,T}$  necessary to deplete the tube. An estimate of the hole density  $p = Q/eL$  can then be obtained by writing the total charge on the tube as  $Q = CV_{G,T}$ .

The NT capacitance per unit length with respect to the back gate (planar surface) is  $C/L \approx 2\pi\epsilon\epsilon_0/\ln(2h/r)$ ,  $r$  the NT radius,  $h$  and  $\epsilon$  are respectively the thickness of the oxide layer and the average dielectric constant.

In Eq. (4.1) one can differentiate between two factors of different origins:

- Geometrical: the transconductance is proportional to  $C/L^2$ , a short channel is favorable to enhance it.

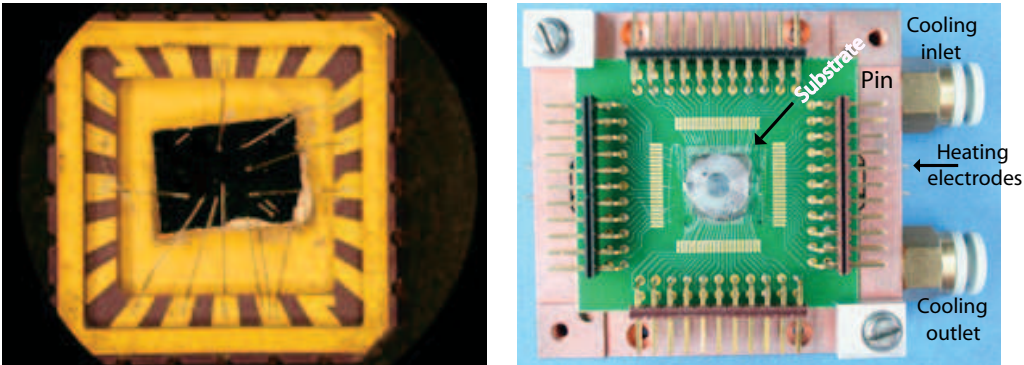


Figure 4.1: FET devices mounted on chip carrier. Left:  $\text{SiO}_2$  substrate, right: quartz substrate, the chip is additionally mounted on temperature system controller (Sec. 5.2)

- Material: the transconductance is proportional to the mobility  $\mu$ . As mentioned in the introduction, The mobility is a function of the lattice vibrations (phonons) and the scattering by the impurities. A material with high mobility is favorable.

## 4.2 Device Fabrication

### 4.2.1 Si/ $\text{SiO}_2$ Substrate

A Si/ $\text{SiO}_2$  wafer piece ( $1 \times 1 \text{ cm}^2$ ) with pre-deposited alignment markers (Chromium) is seeded with nanoparticle catalyst and inserted into the oven for CVD growth (chapter 2). A scanning Electron Microscope (SEM) (LEO - Supra 35, less than 1 kV acceleration voltage) is used to locate the randomly grown tubes. An individual tube according to its length (few microns) and geometry (the straightest and thinnest) is selected with respect to the alignment marks. A layer of polymethylmethacrylate (PMMA) resist is spun over the wafer. Electron Beam Lithography (EBL) (Jeol JSM-IC848 SEM, 35 kV acceleration voltage) is used to pattern the contact structure into the resist. The exposed PMMA is then removed with a developer (MibK (Methylisobutyl-ketone):IPA (Isopropanol) 1:3) and rinsed with IPA after about 50 seconds to stop the development. The metal deposition (usually Pd) has been done by electron beam evaporation in a Balzers PLS 500 system. The

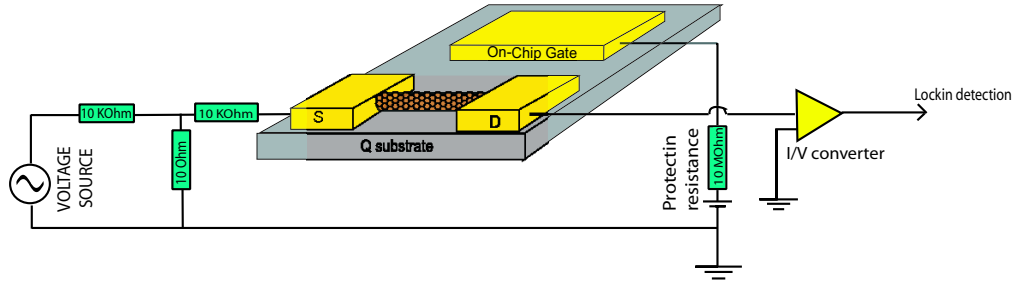


Figure 4.2: Electrical measurements setup for CNTFET on quartz

sample was cooled ( $0^\circ\text{C}$ ) during evaporation to limit the surface diffusion of the metal while evaporation (hit and stick mechanism). An AFM picture of a device is shown Fig. (4.3). A finished device is mounted in a commercially available chip carrier (Fig. 4.1) and contacted with an ultrasonic bonder.

#### 4.2.2 Quartz Substrate

Devices are fabricated on quartz with the following method: negative Ultra Violet (UV) resist (ma - 415) is spun on the top of a ( $2 \times 2\text{ cm}^2$ ) quartz substrate. Alignment markers (Cr) are made by a first step Ultra Violet Lithography (UVL). A second UVL step is made to open small islands that will harbor  $5\text{\AA}$  of evaporated iron (the catalyst). After the CVD growth, a last UVL is performed to define the contact pads (layer of few  $\text{\AA}$  of Cr as anchor and  $40\text{ nm}$  of Pd on top). The contacting pads are defined blindly and a confirmation of a single tube bridging between the electrode is brought after electrical measurement by AFM investigations (Fig. 4.5). The finished device is mounted in a commercially available chip carrier (Fig. 4.1).

### 4.3 Room Temperature Characteristics

Electrical measurement of our devices were performed as a two terminal DC measurements. One electrode is biased with a voltage, and the other is set to the ground via a current voltage convrtter. A DC voltage is applied to the back gate to change the electrostatic potential of the tube.

The set up consists of a lock in amplifier *SR830* Stanford and a home made

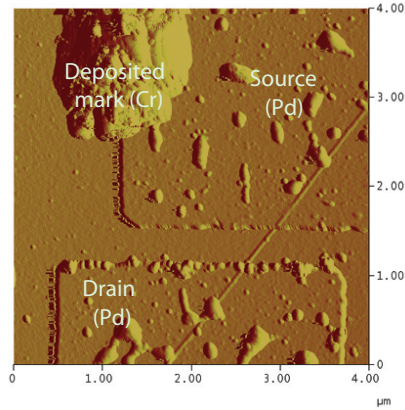


Figure 4.3: AFM picture of a contacted NT on the top of Si/SiO<sub>2</sub> substrate. Apparent height is  $< 2 \text{ nm}$

I/V converter. A data acquisition board is used for fast acquisition measurements. A schematic of the setup<sup>1</sup> is shown in Figure 4.2.

### 4.3.1 Si/SiO<sub>2</sub> FET

The gate response of a device is shown in Figure 4.4(a) At  $V_g=0$ , the device conductance is such that  $G/G_0 = 0.01$ , where  $G_0 = \frac{2e^2}{h} = 7.75 \cdot 10^{-5} \text{ S}$  is the quantum conductance. For large negative voltages, the conductance is higher, the system is in the on state. For large positive voltages, the conductance is low, the tube is depleted and the system is in the off state. At intermediate voltages, the resistance is non linear. This behavior is similar to a p-channel metal oxide semiconductor FET: the carbon nanotube operates as a field effect transistor with holes as a majority carriers.

The origin of p-type character is argued to be inherent to the NT [26] due to doping by the adsorption of atmospheric oxygen (charge transfer)[9, 27]. The other possibility is that the higher work function of the metal leads to an electron transfer from the NT to the contacts [28]. This hypothesis of contact impeding transport is also supported by [32, 33, 34, 35]. However, the discussed devices have resistances in the range of 1–100  $M\Omega$ , i.e. are

<sup>1</sup>For devices on Si/SiO<sub>2</sub> the on chip gate is replaced by a back gate

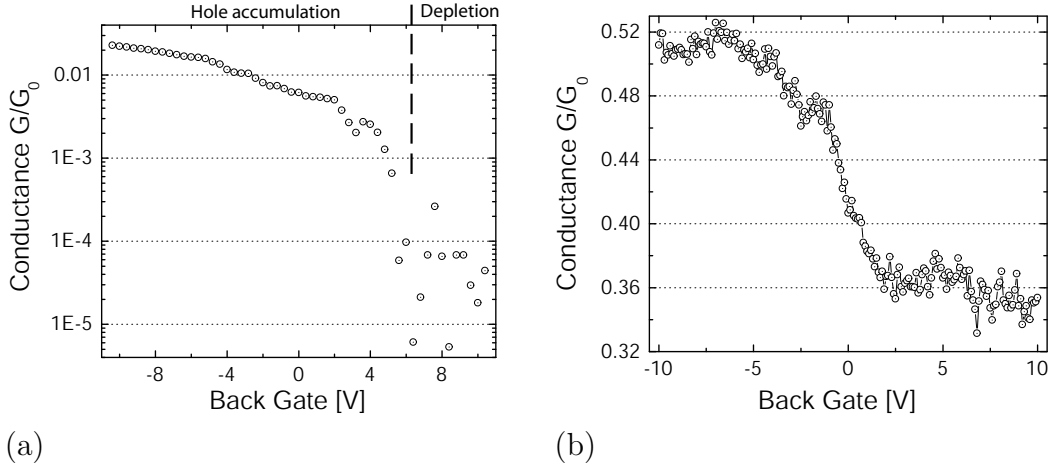


Figure 4.4: (a) Single wall carbon nanotube gate response. (b) Multi wall carbon nanotube gate response

rather high ohmic. Our devices do have a lower resistances.

The one dimensional hole density  $p$  and the mobility can then be estimated. From Eq. 4.1, taking  $V_{G,T} = 6.4$  V. we obtain  $\frac{1}{V_{SD}} \frac{dI}{dV_G} = 8.10^{-8} A/V$ , taking  $h = 400$  nm,  $r = 1.5$  nm,  $\epsilon = 2.5$  and  $L = 500$  nm, the geometrical factor  $C/L^2 = 4.6.10^{-5}$  F.m $^{-2}$ , witch gives a mobility of  $\approx 18$  cm $^2$ /Vs. Note that this estimate results in lower bounds because of (the unknown) contribution to the total resistance from the contacts.

This value is considerably smaller than the  $10^4$  cm $^2$ /Vs observed in graphite [29]. The low value of the NT mobility is consistent with our initial assumption of diffusive transport and suggests that the SWNT contains a large number of scatterers, possibly related to defects in the NT or disorder at the NT/gate - oxide interface due to roughness of SiO $_2$  surface. SWNTs conform to the topography of the surface so as to increase their adhesion. Such deformations can lead to local electronic structure changes, which may act as scattering centers [30].

The CNTFET we have described is an ideal device, for which we supposed that the contacted tube is a single wall. Sometimes, the contacted devices in our experiments could also be a double (or more) wall CNT instead, but with an apparent AFM diameter smaller that 2 nm (Sec. 1.4). Measurements of

such a device is shown on Fig. 4.4(b)

The total resistance  $R_T$  of the device is the sum of the quantum contact resistance (drain and source contacts) and the resistance of the NT itself (scatterers):  $R_T = 2R_C + R_{NT}$ . The contact resistance of this device is  $32 k\Omega$ , just above the quantum contact resistance. This value corresponds to a high transparency (Eq. 2.21) contacts and therefore to high crystallinity tube (nearly no defects).

Ideally the conductance vanishes at higher gate voltages (off state) which is not the case. The nanotube displays a remaining leakage resistance. We suppose therefore that we are measuring a double wall CNT with outer metallic shell and inner semiconducting one. The weak gate response support this hypothesis as the strong electrical screening of the metallic outer most shell prevent an efficient capacitive coupling.

The gate response is one experimental test to know about the nature of the NT (metallic or semiconductor). This is can be complemented by the saturation current the NT can undergo before irreversible damaging. This saturation current is known to be around  $20 \mu A$  per shell [31]. The saturation current is an indication of the quality of the NT, the less defects the tube contains, the larger the saturation current is. In Appendix 2, we show an example of the behavior of two different tubes while undergoing increasing current intensity. The break-down current was found to be about  $18 \mu A$ .

### 4.3.2 Quartz FET

The output characteristics  $G$  versus gate of a single carbon nanotube is shown in Fig. 4.6. corresponding to two different devices. The gate response is non-linear similarly to Si/SiO<sub>2</sub> NTFET.

As in the case of Si/SiO<sub>2</sub> CNFET, we can estimate the value of the mobility (Fig. 4.6(a)) taking  $h = 20 \mu m$ ,  $r = 1.5 \text{ nm}$  and  $L = 4 \mu m$ , the geometrical factor  $C/L^2 = 1.25 \cdot 10^{-6} \text{ F.m}^{-2}$  and  $\frac{1}{V_{SD}} \frac{dI}{dV_G} = 6.2 \cdot 10^{-7} \text{ A/V}$  the mobility  $\mu \approx 500 \text{ cm}^2/V.s$ .

This value is higher than that we previously observed for Si/SiO<sub>2</sub> CNFET although we have longer tube containing a priori more defects. The fact that the interaction tube - substrate can play an important role in scattering phenomena in the tube suggest that this tube interact differently with SiO<sub>2</sub> surface than with quartz surface and this interaction is actually in favor of

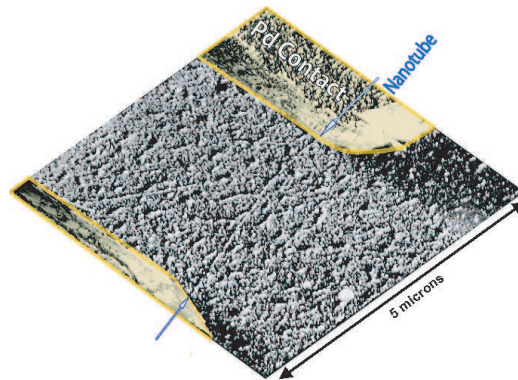


Figure 4.5: AFM picture of a contacted NT on quartz substrate. Apparent height is  $< 2$  nm

scatterers generation in case of  $\text{SiO}_2$  surface.

Figure 4.6(b) shows a gate response with a change of the type of transport. Starting from high negative voltage the conductance decreases indicating p-type behavior. Above 0V the conductance increases indicating an n-type transport this time. The low conductance region suggest a carrier depletion: The tube displays an *ambipolar* behavior.

## 4.4 Conclusion

Field effect transistors could be realized on both quartz and  $\text{Si}/\text{SiO}_2$  substrates using two different gate techniques. The use of the two substrates do have different application possibilities. CNTs on  $\text{Si}/\text{SiO}_2$  can be real basic component for near future nanoelectronic as an example, whereas CNTFET using quartz can have applications for electro-optical measurements in single molecular sensing.

For all this type of applications one has to understand better the physics of transport of carbon nanotubes by controlling the contacts and the surface effects.

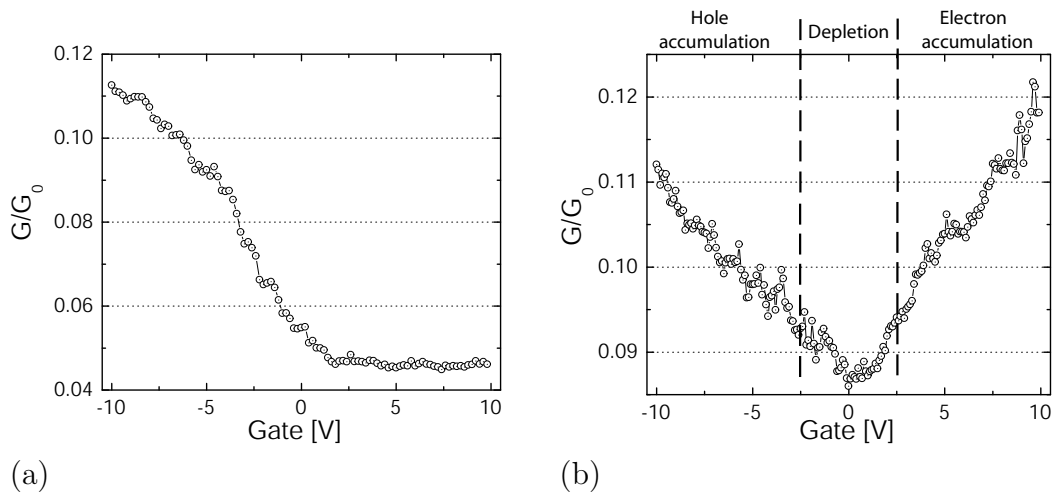


Figure 4.6: (a) p-type behavior of a single carbon nanotube. (b) The graph shows a change of the type of transport from p to n.

# Chapter 5

## *Carbon Nanotubes in Liquids*

In the last chapter (Sec. 4.1), we mentioned that one way to enhance the CNTFET transconductance is to act on the geometrical factor  $C/L^2$ . Reducing the distance between the tube and the gate is one solution. Ideally, the gate electrode could be brought into ultimate contact with the nanotube. In this section we will study the behavior of a nanotube in liquid environment. We will see how the environment can be exploited to enhance the CNTFET performances. The effect of various liquids on the NT will be explored.

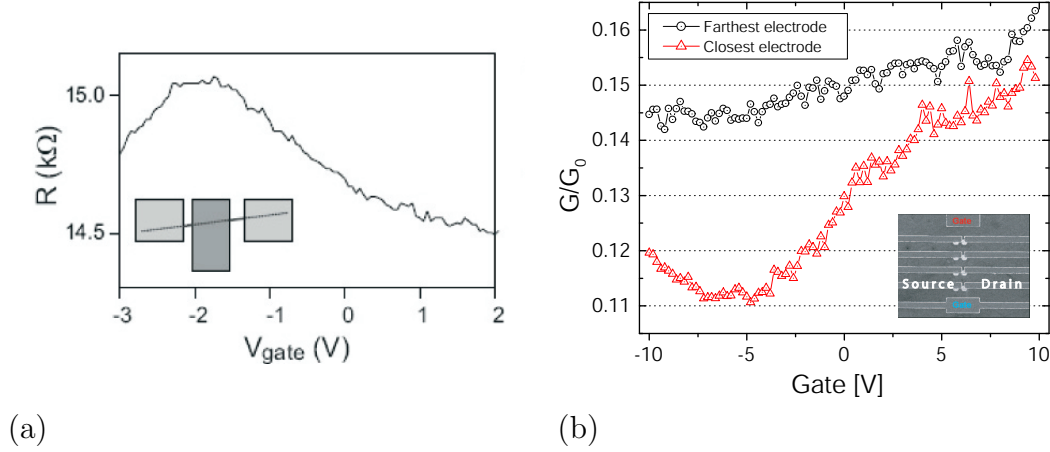


Figure 5.1: (a) Resistance versus  $V_g$  for a MWNT. Al gate (see schematics) is evaporated on top. The width of the Al gate is 500 nm [36]. (b) gate response of a side gate electrode, the picture shows the position of the two gate relative to the source - drain electrodes.

## 5.1 Unconventional Gating

Traditionally, adjusting a dielectric behind a semiconducting structure is called back gating. The back - gate (BG) we used so far is applied via a  $SiO_2$  400 nm thickness. This thickness provides quite a reasonable device yield (the yield is limited principally by leakage to back gate). The transconductance can be increased by reducing the dielectric thickness but the drawback would be the current loss that will take place by leakage. Seeking for new methods to gate a FET is necessary.

### 5.1.1 Planar Gates

- Top gate

A manner to bring a gate as closest as possible to a tube is to place an electrode directly on top. This can be realized by evaporating an aluminium gate separated from the nanotube by a few nanometers of aluminium oxide  $Al_2O_3$  that form during evaporation (pressure of the order of  $10^{-7}$  mbar) by reaction of the aluminium with oxygen residues or water on the tube [36].

An example of the top gate effect is shown in Fig. 5.1(a). The gate is indeed taking effect on the tube. Similar gate was used by Wind *et al* by evaporating Al or Ti on top of a thin oxide with a significant improvement of the transconductance [37].

This method is suitable for instance in low temperature measurements.

- **Side gate**

Lithographically patterned electrodes integrated on the chip surface are fabricated to effectively gate CNFET devices. Fig. 5.1(b) shows that this side gate operates in air and is effectively distance dependent. In the next section, we will see how we can exploit this way to gate a tube with high efficiency.

### 5.1.2 Electrochemical Gate

Krüger *et al* showed that an electrolytic wire like gate is more effective than the conventional backgate geometry [38]. The drawback to the "tip" gate geometry lies in the fact that an *external* tip like electrode is required to gate the devices by immersion into an electrolyte.

We have measured the gate response of semiconducting nanotubes in presence of an electrolyte solution using a *side gate integrated* electrode. A small droplet of a solution 0.1 M NaCl is placed over the device. The droplet size is chosen such that the macroscopically large bonding pads are not immersed in the liquid resulting in negligible leak currents in the resistance measurements. The gate potential is applied via an electrode placed 20  $\mu\text{m}$  away from the device.

Fig. 5.1(b) shows two curves comparing the back gate and the liquid ionic gate. The gating sweep is done between -200 mV and 200 mV to avoid any electrochemical reaction during measurements.

The slopes of the two gate response are about 0.0025 S/V for the back gate and about 0.31 S/V for the electrochemical gate. The liquid gating is approximately 100 more efficient than the back gating which represent also an enhancement of the transconductance.

The reason behind this enhancement is simple. When a voltage is applied to the gate (say positively), the negative solvated ions accumulate along

the surface of the electrode. The nanotube-electrolyte interface is positively polarized. A gate capacitance  $C_g$  takes place due to the the double layer effect (Fig. 5.2(a)). In the Helmholtz picture , the double layer is composed of two rigid planes of charges, the outer Helmholtz plane, being due to the ions with their solvating molecules, the other being that on the nanotube. The electrostatic capacitance  $C_e$  between the tube and ions is given by [39] :

$$C_e = \frac{2\pi\epsilon\epsilon_0}{1 + \ln(2\lambda/d)}$$

where  $\lambda$  is the screening length and  $\epsilon$  the dielectric constant of the water  $\epsilon_{H_2O} = 80$ .

Taking  $\lambda = 1$  nm, an estimation of the value of  $C_e$  is of the order of  $7 \cdot 10^{-9}$  F/m. This value is more than 2 order of magnitude larger than the back gate capacitance  $\sim 10^{-11}$  F/m taken from Coulomb - blockade measurements [40, 41]. The total capacitance, which relates the electrochemical potential difference applied between the tube and the gate to the charge of the tube has both electrostatic and quantum (chemical)  $C_Q = e^2 g(E)$  [42] where  $g(E)$  is the density of states for the CNT. The density of state (1D tube) is given by:

$$g_E = \frac{4}{\pi\hbar v_F} \frac{\sqrt{E^2 - E_g/2}}{E}$$

The quantum capacitance is therefore of the order  $C_Q = \frac{4}{\pi\hbar v_F} \sim 10^{-10}$  F/m. For the case of back gate the smallest capacitance dominates the overall capacitance. In liquid gating, on the other hand, the quantum capacitance dominates.

The possibility of having a FET with high transconductance (ultimately with a ballistic nanotube) makes it capable for molecular sensing of single molecule. A charged molecule will act as an effective gate changing, the conductance of the tube.

## 5.2 Carbon Nanotube in an Organic Solution

The common methods to gate a metal-oxide semiconductor (MOSFET) structure can be electrical (previous section) or chemical. Chemical gate \*consists\* reside in that the resistance can change when species adsorbs in the

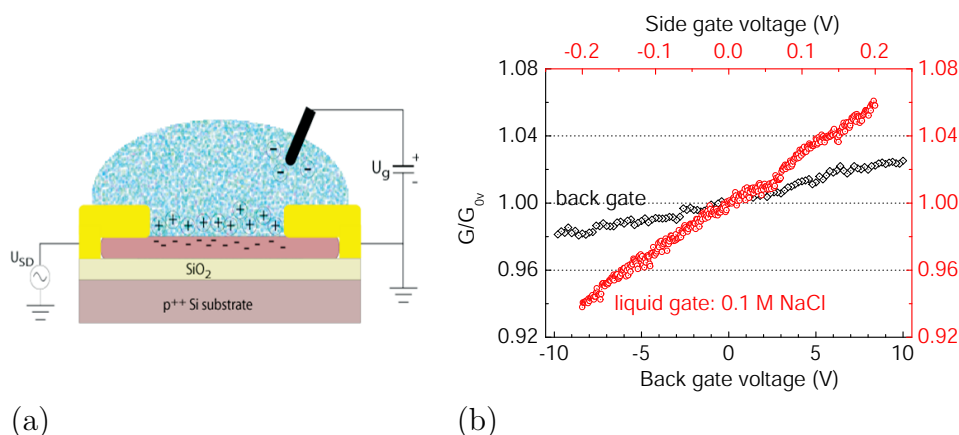


Figure 5.2: (a) Liquid gating schematic. The ions are in contact with the tube. (b) Response of the NT to ionic gating. The conductance is normalized by its value at zero gate voltage.

semiconductor surface. Adsorption of atmospheric oxygen on the surface as an example, dissociate to form  $O^-$ , where the electron is extracted from the semiconductor. This electron extraction tends to increase the resistance (assuming an n-type semiconductor).

The property of modulating a resistance via an external chemical agent can be a way of detecting the chemical agent itself. The built-in amplification of a CNFET can be responsible of a big resistance change while chemically ‘perturbing’ the surface states. A transduction of the chemical action is hence possible with high sensitivity.

The sensitivity is defined as the ratio of the change in sensor output to the change in the value of the quantity we aim to measure (adsorbate electronegativity, degree of oxidation, etc...). This depends on the built-in amplification or the transconductance in our case. Enhancing the transconductance is important to increase the sensitivity of a Chemical CNTFET (ChemCNTFET).

### 5.2.1 NT in Aromatic Compound

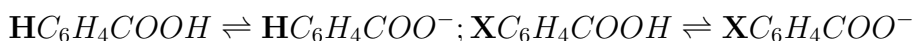
Aromatic compounds are known to interact strongly with the  $\pi$ - $\pi$  bonds of graphitic walls of SWNTs [43]. These interactions manifest themselves in the

solubilization of SWNTs in aromatic solvents [44] as well as solubilization in solutions of certain aromatic surfactants and polymers [45].

### Aromatic compound and structures constant

It is known in organic chemistry that common functional organic group compound enable the same reactivity (aromatic, carboxylic acids, etc). The effect of the side group, in some case, does not influence the reaction but rather the rate or the position of equilibrium (formic acid  $\text{HCOOH}$  has  $pK_a = 3.77$ , carboxylic acid  $\text{CH}_3\text{COOH}$  has  $pK_a = 4.72$ ). The effect of the side group (the structure) on the reactivity can be modelled by inductive<sup>1</sup>, steric<sup>2</sup> or *resonance* effect (Appendix. 7.3.2). Quantitatively, this treatment is done by the so called Hammett formalism [46].

Suppose that  $\text{HC}_6\text{H}_4\text{COOH}$  and  $\text{XC}_6\text{H}_4\text{COOH}$  ( $X$  is an *arbitrary* side group) have equilibrium constants of  $k_0$  and  $k_X$  for the two reactions:



the Hammett equation is defined by:

$$\log \frac{k_X}{k_0} = \sigma$$

The constant  $\sigma$  is therefore characteristic of the group  $X$ . It represents the ability of this group to withdraw or donate electron density by combination of its inductive or resonance effect. This quantity is called Hammett or structure constant and it can be evaluated experimentally by thermodynamic measurements or numerically by quantum calculation.

The set of values  $\sigma$  sum up the total electrical effects (resonance plus inductive) of a group  $X$  when attached to a specific functional group (exp: benzene). A positive value of  $\sigma$  indicates an electron-withdrawing group and a negative value, an electron-donating group. The table below gives the values of  $\sigma$  with the dipolar moment of the molecule for different side groups

<sup>1</sup>Caused by polarization of the bonds. This effect is larger when increasing the substituent electronegativity for instance.

<sup>2</sup>Steric effect is related to influence of the size of the substituent on the reaction rate.

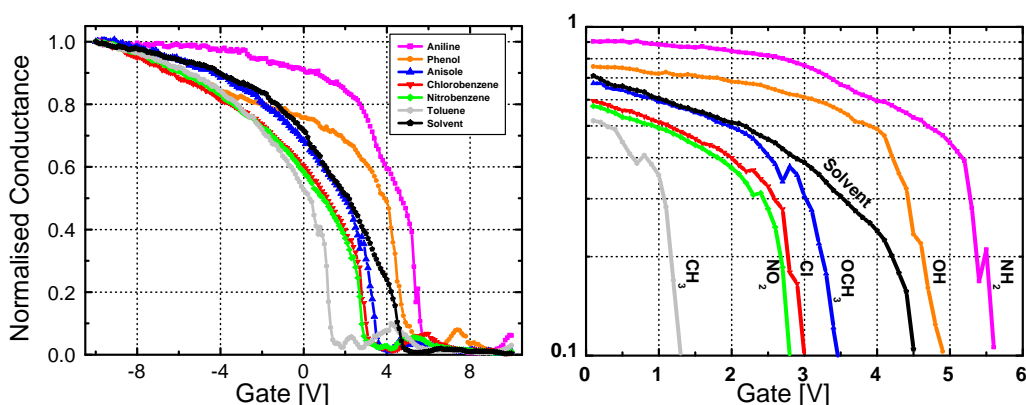


Figure 5.3: Normalized conductance versus back gate of different compounds. The right plot is a zoom in region from 0 to 6 V.

when attached to a benzene ring.

	$NH_2$	$OH$	$OMe$	$Me$	$H$	$Cl$	$NO_2$
Hammett constant	-0.66	-0.36	-0.27	-0.17	0	0.23	0.78
$\mu$ (Debye)	1.13	1.22	1.38	0.37	0	1.69	4.22

### NTFET in aromatic

$X-C_6H_5$  ( $X$ :  $NH_2$ ,  $OH$ ,  $OCH_3$ ,  $NO_2$ ,  $CH_3$  and  $Cl$ , corresponding to aniline, phenol, anisole, nitrobenzene, toluene and chlorobenzene) are dissolved in cyclohexane 0.2 M. A small volume is applied to the device fabricated on  $Si/SiO_2$  substrate.

For each liquid application, a forward and backward scan between -10V and 10V with a scan rate of 0.1V and dwell time of 100 ms. The back and forward scan is maintained until the curves become stable. Between liquid exchange, the sample is cleaned thoroughly with isopropanol and chloroform (appendix 7.3.1).

Fig 5.3. shows the back gate response with every compound  $X - C_6H_5$ . The p-type semiconductor behavior is *conserved* with all products with different decreasing slopes. The turn-off voltage (taken at  $G = 0.1 \cdot G_{max}$ ) shifts

relatively to the solvent by  $\Delta V_g = V_g(X)$  depending on the substituent X.

In order to understand the interaction mechanism of aromatic with CNTs, we plot the gate shift versus the Hammett constant  $\sigma$ . Fig 5.4 (a) shows this dependence. The gate shift follows a linear law in agreement with [43]. The deviation for toluene is explained by a difference of the adsorption mechanism taking place on the tube surface. In fact, Methyl does not have an external *unshared* electron pair like all other aromatic explored here ( $-\bar{N}H_2$ ,  $-\bar{Cl}$ , etc...). This pair is directly conjugated to the double benzyl bond and participate to electron *delocalization* [47]. This delocalization is displayed as different mesomere of the compound (Appendix 7.3) and the NT-aromatic interaction is related to it.

The description of the NT-aromatic in terms of the Hammett constant is more subtle than just a simple dipole-NT interaction. The Hammett constant includes the way the charges are organized around the molecule. The sensitivity of the tube goes beyond a simple dipolar response to give an idea about the organization of the external electronic cloud around the molecule.

From the linear approximation, zero shift (and correspondingly no charge-transfer between aromatic compound and nanotube) correspond to finite negative value of sigma which is an indication of the presence of donating contaminants in the tube surface.

The macroscopic effect of the charge transfer is manifested as a shift of the gate response. The microscopic origin of this shift is related to the mobility of the charge carriers in the semiconducting tube. In non polar semiconductors, the mobility is determined by the interaction with acoustical vibrations (phonons) of the lattice as well as by scattering by impurities or other lattice defects as mentioned before. The adsorption of an aromatic compound with different valence electronic configuration will induce different local distortions of the electronic structure of the tube influencing hence the mobility.

In analogy to what has been suggested for gas sensitivity in air [9], It is conceivable to suppose that the mobility change is the result of charge transfer between the NTFET device and the aromatic molecules adsorbed onto the carbon nanotube conducting channel. Fig. 5.4(b) plot the relative mobility change  $(|\mu_X - \mu_{ref}|)/\mu_{ref} = \Delta\mu/\mu$ , where  $\mu_X$  and  $\mu_{ref}$  are the mobilities in presence of the compound X and the solvent only. This quantity reflects

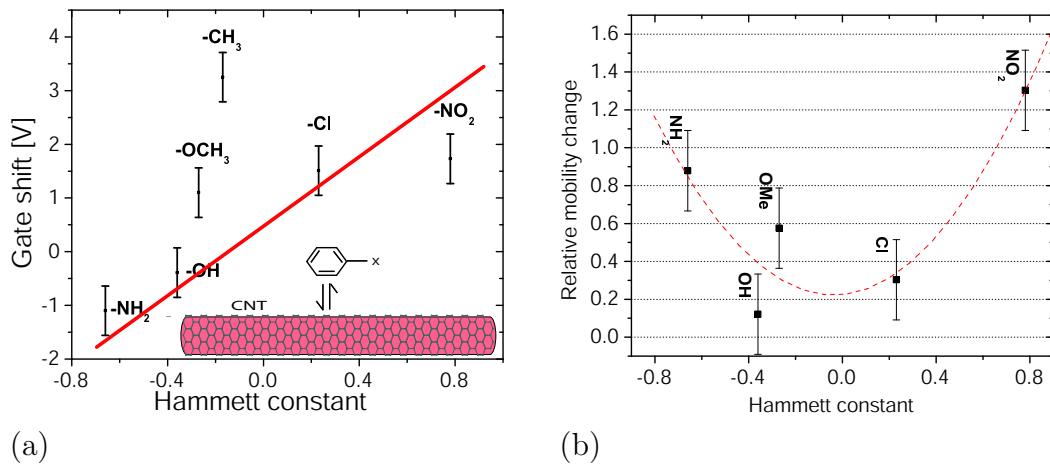


Figure 5.4: (a) Behavior of the gate shift to the Hammett constant for different side groups, the continuous line is a linear approximation. (b) Relative mobility change  $\Delta\mu/\mu$  versus Hammett constant, the dashed line is a quadratic function plotted for eye guidance.

the magnitude of output change to the change of the external excitation or the "measurand" (Hammett constant in our case). The biggest perturbation is induced by the nitrobenzene due to its strong donating electrons capability. The smallest constant is that of chlorobenzene and the nanotube is still sensitive to it. For practical applications, perturbations are amplified by the built-in amplification of the CNTFET.

The non linear approximation (dashed curve) of the relative mobility change in the Fig. 5.4(b) suggests that the perturbation of the overlap  $\beta$  is non linear at least for high  $\sigma$  values. For a mono-atomic infinite chain we know that the energy is proportional to the overlap resulting in a mobility also proportional to the overlap. The fact that the tube is not a pure 1-D infinite system and eventually that the adsorbate can not be totally removed after cleaning steps can result for such non - linearity.

### 5.2.2 NTFET in Liquid Crystal

We have studied so far the behavior of a nanotube in different class of liquids. We have seen that the tube is sensitive to an electrolyte, which is a solution of

a totally dissociated molecules (anions + cations), and to aromatic representing a class of neutral molecules. We will explore another system: molecules carrying a finite dipolar moment represented here by a liquid crystal.

### Dipole orientation

It is well known that the liquid crystal (LC) is a state of matter which has partial order. This order is governed by the dipolar interactions and thermal fluctuation that tends to destroy it. In the presence of a *homogenous* electrical field the LC will tend to have order corresponding to the minimal energy configuration.

### Orientalational gating

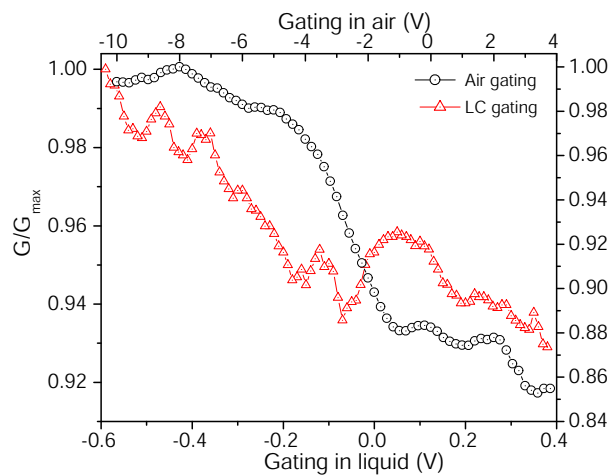


Figure 5.5: Gate response in air and in presence of the liquid crystal.

A droplet of MBBA (N-(p-methoxybenzylidene)-p-butylaniline), a nematic liquid crystal, is applied on a device fabricated on a quartz substrate. The measurements were carried out using a special holder shown in Fig. 4.1. This holder was built in the perspective to heat the system above the critical transition temperature order-disorder (Appendix 7.4).

We use a side gate and the measurements were realized at room temperature where the liquid crystal is in its *ordered* state. Fig. 5.5. shows the gate

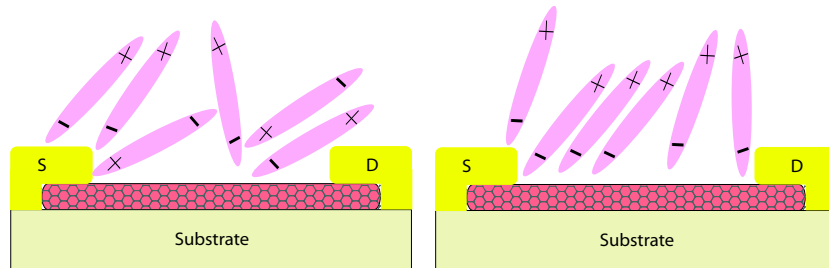


Figure 5.6: Random dipolar orientation on the right, partially ordered dipoles on the left. The disorder can be induced by thermal fluctuations or in presence of inhomogeneous electrical field

response of the nanotube in air and in liquid. A gate effect is clearly seen and at this time, the liquid gating is only about seven time more efficient than the air side gating. This weak effect is understandable as we are only gating via dipoles (partial charge).

The carbon nanotube is sensitive to the dipolar moment carried by the liquid crystal molecules. The effect of an increasing electrical field is to align or orient the LC dipoles influencing hence more and more the tube.

### 5.3 Possible Applications

The spectrum of application of carbon nanotube in liquids is very wide. The study of nanotube in electrolyte is important to enhance the performance of CNTFET for nanoelectronic and single molecular sensing. Charge transfer via certain special compound may help to dope selectively a tube towards realizing a p - n junction. The tube imbedded in LC can be a sensitive temperature detector, as the order of the dipoles in the LC influences the conductance of the tube and this perturbation will be amplified by the FET effect. Detecting also the local defect of the tube is possible; a defect represent a local resistance that induces a potential drop inducing a local inhomogeneous electrical field which can disorder the system hence changing the optical properties [49].

# Chapter 6

## *Outlook and Conclusion*

Exploring electrical properties of carbon nanotubes in various media was the main subject discussed here. Carbon nanotubes are one dimensional system with interesting electrical transport properties and chemical stability. Those characteristics can open a wide field of applications, for instance, in molecular sensing. toward achieving this ultimate goal, we grow different type of carbon nanotubes (Chap. 2) and characterize the electrical properties in air of the contacted ones (Chap. 3). In chapter 4, we explore the effect of an electrolyte, a neutral solution and a dipolar solution on the nanotubes. We found that the tube is indeed responding to these environment but differently. This selectively together with the high sensitivity of the tubes makes them a potential molecular sensor for a large variety of liquids.

# Chapter 7

## *Appendix*

### 7.1 Chemical Vapor Deposition Growth Parameters

Catalyst	Temperature	$CH_4$	$C_2H_4$	$H_2$	$Ar$
Iron layer	850	-	20	688	1059
Ferritin	700	-	20	688	1059
Iron particles	950	210	-	-	130

The order of opening different gases is as following: The first two processes the Argon flows until the growth temperature is reached. The hydrogen is introduced for 5 min followed by the hydrocarbon 10 min. For the third process, the Argon is closed and the hydrocarbon flows for 10 min once the grown temperature is reached.

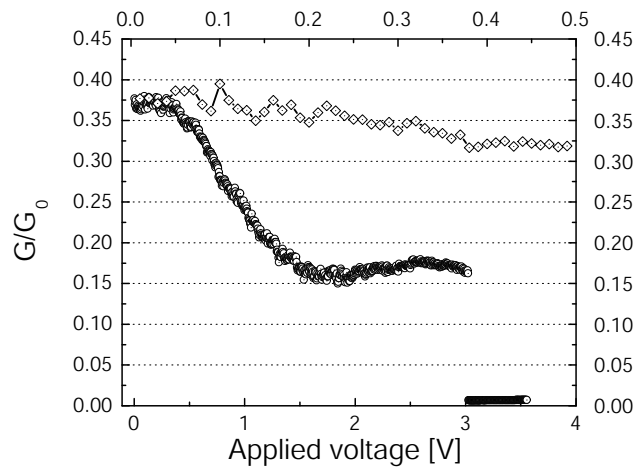


Figure 7.1: Nanotube id destroyed above the threshold current ( $18\mu\text{A}$ )

## 7.2 Shell Burning

The CNTs can support a remarkable large current before electrical breakdown occurs. When the contact resistance is sufficiently low the SWNT present strong non linear response before failing. This interesting feature reflects the strong ability of the tube to rearrange microscopically before total destruction. An example of the electrical breakdown of a SWNT (we believe) is shown in Fig. The applied voltage over the tube could be raised to  $3\text{ V}$  at which the current saturated at a value of  $18\ \mu\text{A}$  (circle curve). The non linear response start around a current value of  $8\ \mu\text{A}$ . The square curve correspond to another device for guidance.

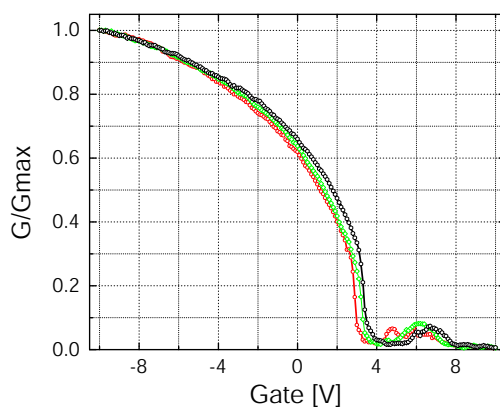


Figure 7.2: Gate response after washing steps with chloroform and cyclohexane

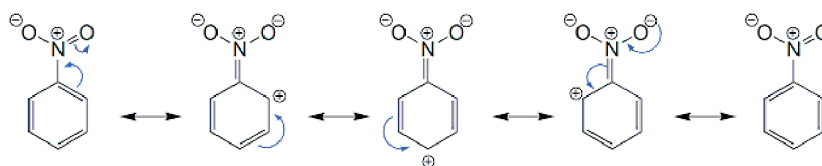
## 7.3 CNFET in Aromatic

### Washing

The Figure 7.2 above display the gate response of the device after washing operations. The adsorbate could be removed as we could get back the initial tube response. The slight voltage difference at  $0.1G_{max}$  is took as an uncertainty for the gate shift. Its due to the remaining adsorbate or some other chemicals present in the solutions because of the finite purity.

### Resonance

Resonance effect: groups which contain an unshared pair on an atom connected to an unsaturated system. Different mesomere form of aniline. The



charge transmission is assured by the conjugation, the transmission is responsible for the charge delocalization.

## 7.4 Additional Liquid Crystal Measurements

We present here the gate response of 5CB (Cholesterol benzoate) liquid crystal to gate for different temperatures. The transition temperature is around  $35^\circ\text{C}$ . For a fixed gate voltage, the conductance decrease while increasing the temperature. The orientation of the dipole above the transition temperature is random influencing less the tube. In the ordered state, the gating is enhanced due to the collective effect of the dipoles.

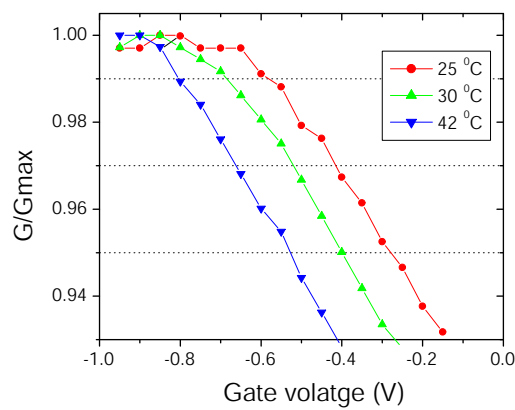


Figure 7.3: Conductance change versus gate voltage for different temperatures

The picture below is represent the polarization effect of the MBBA taken by an optical microscope. We can see the local light contrast difference due to the local light polarization.



# Chapter 8

## *Acknowledgement*

Everything that has a start has an end. It is time to end the period of research apprenticeship by writing the acknowledgement to all people that participate in this work or interact with it; I cite:

The source of funding National Center for Competence and Research (NCCR): thanks from the bottom of my heart.

Christian schoenenberger my advisor: Thanks to you for your scientific help and support.

Michel Calame: Thank you for scientific support and discussions.

Dino Keller : Thanks for help and collaboration. Hope that you will have success in your future research.

The group members: Z. Liu, Mark Buitelaar and Adam hansen who left us at some earlier stage.

Francois dewarrat: thanks for teaching me some of the lab techniques.

By courtesy, I would like to thank mattias Graber, takis Kontos, lucia Gruter, laetitia Bernard and also juerg Furer my room mate and the new group members Jianhui Liao and Ming Wu.

I would like to thank equally and sincerely the social surrounding in basel, I cite: sandra Dececco my best friend in basel, laila Ifadir my sister, the white men david Oppenheim and my master advisor Francois Graner.

I am also grateful to this country which gave me the opportunity to do my PhD here.

In the memory of my father the big and persistent worker.

Finally, I thank God, creature of the universe, for giving me the heart and the mind to appreciate the beauty of the world ...

# Bibliography

- [1] H. W. Kroto, J. R. Heath, S. C. OBrien, R. F. Curl, R. E . Smalley, *Nature*, 318, 162, (1985).
- [2] S. Iijima, *Nature*, 354, 65, (1991).
- [3] R. L. Jacobsen, T. M. Tritt, J. R. Guth, A. C. Ehrlich, D. J. Gillespie, Mechanical properties of vapor-grown carbon fiber, *Carbon*. 391, 59 (1998)
- [4] A. T. Johnson, M. Freitag, M. Radosavljevic and S.V. Kalilin, and D.A. Bonnell, *Inter. Jour. Nanosci.*, 1, 247, (2002).
- [5] A. G. Rinzler, J. H. Hafner, P. Nikolaev, L. Lou, S. G. Kim, D. Tomanek, D. Colbert and R. E. Smalley, *Science*, 269, 1550, (1995).
- [6] A. C. Dillon, K. M. Jones, T. A. Bekkedahl, C. H. Kiang, D. S. Bethune and M. J. Heben, *Nature*, 386, 377, (1997).
- [7] H. Dai, J. H. Hafner, A. G. Rinzler, D. T. Colbert and R. E. Smalley, *Nature*, 384, 147 (1996).
- [8] V. Derycke, R. Martel, J. Appenzeller and Ph. Avouris, *Appl. Phys. Lett.*, 80, 2773, (2002).
- [9] P. G. Collins, K. Bradley, M. Ishigami, A. Zettl, *Science*, 287, 1801, (2000).
- [10] J. Kong, N. R. Franklin, C. Zhou, M. G. Chapline, S. Peng, K. Cho, H. Dai, *Science*, 287, 622, (2000).
- [11] P.R Wallace, *Phys. Rev*, 71, 9, (1947).

- 
- [12] R. Saito, G. Dresselhaus, M.S. Dresselhaus: Physical Properties of Carbon Nanotubes (Imperial College Press, London, 1999).
- [13] J. W. G. Wildöer, L. C. Venema, A. G. Rinzler, R. E. Smalley and C. Dekker, *Nature*, 391, 59 (1998).
- [14] A. P. Sutton: Electronic Structure of Materials (Oxford Science Publication, New York, 1994).
- [15] A. Thess, R. Lee, P. Nikolaev, H. Dai, P. Petit, J. Robert, C. Xu, Y. H. Lee, S. G. Kim, A. G. Rinzler, D. T. Colbert, G. E. Scuseria, D. Tomanek, J. E. Fischer, R. E. Smalley, Crystalline ropes of metallic carbon nanotubes, *Science*, 273, 483, (1996).
- [16] M. J. Yacaman, M. M. Yoshida, L. Rendon, J. G. Santiesteban, Catalytic growth of carbon microtubules with fullerene structure, *Appl. Phys. Lett.*, 62, 202, (1993).
- [17] V. N. Popov, *Mat. Sci. Eng.*, 43, 61, (2004).
- [18] Ph. Mauron, *Growth Mechanism and Structure of Carbon Nanotubes*. PhD thesis, Universität Freiburg, 2003.
- [19] S. Ohnishi, M. Hara, T. Furuno, H. Sasabe. *Biophys. J.*, 63, 1425, (1992).
- [20] C. A. Johnson, Y. Yuan, A. M. Lenhoff *J. Colloid. Interf. Sci.*, 223, 261, (2000).
- [21] R. T. K. Baker, Catalytic growth of carbon filaments, *Carbon*, 27, 315, (1989).
- [22] S. Amelinckx, X. B. Zhang, D. Bernaerts, Z. F. Zhang, V. Ivanov, J. B. Nagy, A formation mechanism for catalytically grown helix shaped graphite nanotubes, *Science*, 265, 635, (1994).
- [23] Y. Zhang, Y. L. Kim, D. Wang, H. Dai. *Appl. Phys. A*, 74, 325, (2002).
- [24] Picture treated with WSxM; <http://www.nanotec.es>.
- [25] J. M Bonard, J. P. Salvetat, T. sctoeckli, W.A. de Heer, L. Forro, A. Chatelier, *App. Phys. Lett.*, 73, 918, (1998).

- 
- [26] R. Martel, T. Schmidt, H. R. Shea, T. Hertel, Ph. Avouris, *App. Phys. Lett.*, 73, 17, (1998).
- [27] G. U. Sumanasekera, C. K. W. Adu, S. Fang, and P. C. Eklund, *Phys. Rev. Lett.*, 85, 1096, (2000).
- [28] S. J. Tans, A. R. M. Verschueren, and C. Dekker, *Nature*, 393, 49 (1998).
- [29] N. B. Brandt, S. M. Chudinov, and Ya. G. Ponomarev, *Semimetals, Graphite and its Compounds*, ( North-Holland, Amsterdam, 1988).
- [30] R. Martel, T. Schmidt, H. R. Shea, T. Hertel, and Ph. Avouris *App. Phys. Lett* ,73, 2447, (1998).
- [31] P.G. Collins, Ph. Avouris, *App. Phys. A*, 74, 329, (2002).
- [32] N. B. Heinzet, S. M. Tersoff, and Ya. G. Martel, Derycke, Appenzeller J and Avouris, *Phys. Rev. Lett* ,89, 106801-1, (2000).
- [33] Martel R, Derycke V, Lavoie C, Appenzeller R, Chan K K, Tersoff J and Avouris, *Phys. Rev. Lett* , 87, 256805, (2000).
- [34] M. Freitag, M. Radosavljevi, Y. Zhou and A. Johnson *Appl. Phys. Lett.*, 79, 3326, (2000).
- [35] B. Babic, M. Iqbal and Ch. Schönenberger *Nanotech.*, 14, 327, (2003).
- [36] Marc Buitelaar, *Electron Transport in Multiwall Carbon Nanotubes*, PhD thesis, University of Basel, 2004.
- [37] S. J. Wind, J. Appenzeller, R. Martel, V. Derycke and Ph. Avouris, *Appl. Phys. Lett.*, 80, 3817, (2002).
- [38] M. Krüger, M.R. Buitelaar, T. Nussbaumer and C. Schönenberger, *Appl. Phys. Lett.* 78, 1291, (2001).
- [39] S. Rosenblatt, Y. Yaish, J. Park, Gore, V. Sazonorova and P. L. McEuen, *Nano. Lett.*, 2, 869, (2002).
- [40] S. Tans, M. Devoret, H. Dai, A. Thess, R. Smalley, L.J. Georliga, C. Dekker, *Nature*, 386, 474, (1997).

- 
- [41] D. Cobden, M. Bockrath, P. McEuen, A. Rinzler, R. Smalley, *Phys. Rev. Lett.*, 81, 681, (1998).
- [42] R. Luryi, *App. Phys. Lett.*, 52, 501, (1988).
- [43] A. Star, T. R. Han, J. C. P. Gabriel, K. Bradley, and G. Grüner *Nano. Lett.*, 78, 1291, (2001).
- [44] Y. Sun, S. R. Wilson, D. I. J. Schuster *Am. Chem. Soc.*, 123, 5348, (2001).
- [45] J. Liu *et al Science*, 280, 1253, (1998).
- [46] C. Hansch, A. Leo, R. W. Taft, *Chem. Rev.*, 91, 165, (1991).
- [47] J. March: *Advanced organic chemistry*, (McGraw-Hill, 1977). Chap. 2, 9.
- [48] V. Chigrinov, *Mol. Cryst. Liq. Cryst.*, 179, 71, (1990).
- [49] V. Chigrinov, G. Nevskaya, *Mol. Cryst. Liq. Cryst.*, 209, 9, (1991).